

# Steered Molecular Dynamics of an Anticancer Peptide Interacting With The p53 DNA-binding Domain\*

XU Xian-Jin<sup>1)</sup>, SU Ji-Guo<sup>2)</sup>, CHEN Wei-Zu<sup>1)</sup>, WANG Cun-Xin<sup>1)\*\*</sup>,  
CANNISTRARO Salvatore<sup>3)</sup>, BIZZARRI Anna-Rita<sup>3)\*\*</sup>

<sup>1)</sup> College of Life Science and Bioengineering, Beijing University of Technology, Beijing 100124, China;

<sup>2)</sup> College of Science, Yanshan University, Qinhuangdao 066004, China;

<sup>3)</sup> Biophysics and Nanoscience Center, Department of Ecology and Biology (DEB), University of Tuscia, 01100 Viterbo, Italy)

**Abstract** The p28 peptide, derived from the blue copper protein azurin, is known to enhance the anticancer capabilities of the tumor suppressor p53 likely binding to its DNA-binding domain (DBD). The p28-p53 DBD complex has been investigated by steered molecular dynamics in order to characterize the unbinding process at atomic resolution. We found that the unbinding of the complex follows a candidate pathway with a well-defined detaching sequence between the partners. The analysis of the unbinding force and the calculation of the irreversible work done along several unbinding paths have allowed us to extract information on the energy landscape regulating the unbinding process.

**Key words** steered molecular dynamics, p53, anticancer peptides

**DOI:** 10.3724/SP.J.1206.2013.00294

Recent studies have reported that the 28-amino-acid peptide fragment (p28) from the blue copper azurin (aa 50~77), forms a complex with the transcription factor p53<sup>[1-2]</sup>. p53 is a tetrameric protein which is well-known to play a crucial role in preventing cancer growth by maintaining the genome stability<sup>[3-4]</sup>. Indeed, p28 enhances the intracellular levels of p53, which is critical towards the activation of the transcription of downstream target genes regulating DNA repair, cycle arrest and apoptosis, inheriting the overall tumoricidal activity of azurin but with less side effects<sup>[1-2]</sup>. In this respect, the knowledge of the interaction properties between p28 and p53 could be of utmost importance to fully understand the molecular mechanisms regulating the complex formation, even in the perspective of designing new drugs which target the p53 pathway. Since the structure of the p28-p53 complex is not known, we have recently carried out a computational docking

study on the interaction between p28 and the core DNA-binding domain (DBD) in order to obtain information on possible binding sites<sup>[5]</sup>. We have also studied by atomic force spectroscopy (AFS) the unbinding process between the p28 peptide with full-length p53 and with different isolated domains of p53<sup>[6-7]</sup>. Interestingly, we found that p28 binds to the DBD region of p53, in agreement with the docking results, while it does not interact neither with the

\*This work was supported by grants from International S&T Cooperation Program of China (2010DFA31710), The National Natural Science Foundation of China (11204267), The doctoral fund of innovation from Beijing University of Technology and by a grant from The Italian Association for Cancer Research (AIRC No IG 10412).

\*\*Corresponding author.

WANG Cun-Xin. Tel: 86-10-67392724, E-mail: cxwangbjut@gmail.com  
BIZZARRI Anna-Rita. Tel: 39-761-357031, E-mail: bizzarri@unitus.it

Received: June 24, 2013 Accepted: December 9, 2013

N-terminal transactivation (NT) nor with the C-terminal tetramerization (CT) domains<sup>[6]</sup>.

Although AFS has opened new perspectives in the study of biorecognition, it does not however provide any molecular detail on the binding sites and even on the temporal evolution of the unbinding process, which can be instead important to understand the molecular basis of the interaction<sup>[7-8]</sup>. To both investigate these aspects and elucidate the landscape of the unbinding process at molecular level, here we have applied steered molecular dynamics (SMD) to the complex formed by p53 DBD and p28. In SMD simulations, the unbinding of a complex is induced by pulling, at a constant speed, a spring bound at an atom of one partner, while at least one atom of the other partner engaged in the complex is kept fixed<sup>[9-10]</sup>. In such a way, the time evolution of the system during the pulling can be followed at atomic resolution; this enabling to disclose subtle molecular details underlying the unbinding process<sup>[10-17]</sup>. Additionally, the use of suitably theoretical models (*e.g.* Bell-Evans model and Jarzynski's equality), to analyze the SMD nonequilibrium trajectories allows one to obtain information on the energy landscape and on the thermodynamic properties of the complex, at equilibrium<sup>[18-22]</sup>. In particular, SMD has been applied to the p28-p53 DBD complex by pulling a spring bound to the sulphur of the p28 N-terminal while a nitrogen of Lys 139 of p53 DBD is kept frozen. The starting structure of the complex has been chosen from a previous modeling work suitably adapted to mimic the conditions used in the experimental AFS setup<sup>[5-6]</sup>. The results suggest that the complex unbinds mainly following a candidate detaching pathway characterized by a well-defined sequence of the contact points between the partners. Furthermore, we have evaluated the profile of the binding free energy along the reaction coordinate by calculating the potential of mean force (PMF) through the Jarzynski's equality. All these results shed light on the molecular mechanisms regulating the complex formation whose knowledge, in turn, could help for tailoring the peptide molecular structure in order to achieve an enhanced anticancer activity.

## 1 Methods

### 1.1 p29-p53 DBD complex

The initial atomic coordinates of p53 DBD (a domain of one of the four units of p53), were taken

from chain B of PDB entry 1tup<sup>[23]</sup>. As shown in Figure 1, p53 DBD contains a Zn ion forming a Cys3His-Zn motif with Cys176, His179, Cys238 and Cys242 residues. The interaction of the Zn ion with its ligands was treated through a bonded approach. In particular, the Zn-N and Zn-S bonds and S-Zn-S angles, were set according to the parameters provided in the reference<sup>[24]</sup>. Additionally, in Cys3-His-Zn motif, Cys A (from G43a1 Gromacs force field) was used, while Cys B was used for other Cys residues in the complex. His was treated as deprotonated. Since three Cys A residues were used, each one having a charge of  $-0.5e$ , the total charge of the complex is then  $-1.5e$ ; the Zn charge was fixed to  $1.5e$  to guarantee an integer net charge for the protein. The final total charge of p53 DBD is  $3.0e$ . The setting of charges for Cys3His-Zn motif are close to the values of charges calculated with 6-311G\*\* basis set<sup>[24]</sup>.

The structure of p28, a 28 amino acids fragment from Azurin (Leu50- Asp77), in solution was derived by submitting the related portion from Azurin to a long time molecular dynamics (MD) simulation<sup>[5]</sup>. The resulting structure exhibits an  $\alpha$ -helix, partially coincident with that of Azurin and the N- and C-terminals coupled through a  $\beta$ -sheet forming a loop. In the present work, a Cys residue was added to the N-terminal of p28 using SPDBV 4.02<sup>[25]</sup>. p28 then becomes p29 and the sequence of p29 being then renumbered from Cys1 to Asp29. Such a change was done to make our SMD system closely similar to the AFS experimental setup, in which p29 was linked to the AFM silicon nitride tip through the thiol group of the added Cys residue (see also below)<sup>[6]</sup>; the final charge of p29 being  $-4.000e$ . Finally, the structure of p29-p53 DBD complex was taken from the best model obtained in a previous related modeling work, adapted to include the addition of the Cys residue to p28<sup>[5]</sup>. The final charge of the complex was then  $-1.000e$ . Such a model was derived by analyzing a deep analysis of several docking models in terms of the binding free energy, the shape complementarity, the number of stabilizing hydrogen bonds, the polar interface character, the engaged aminoacid residues, etc. The selected best model is indeed characterized by both the lowest binding free energy and high scores for interface properties.

### 1.2 MD simulations

The MD simulations of the p29-p53 DBD complex were performed by using GROMACS 4.0.5<sup>[26]</sup>

with the G43a1 force field<sup>[27-28]</sup>. Bond lengths were constrained by the LINCS algorithm<sup>[29]</sup>. The velocity rescaling method<sup>[30]</sup> was employed to maintain the temperature at 300 K, and the Parrinello-Rahman approach<sup>[31]</sup> allowed us to maintain the pressure at 1 atm. The time constants for temperature and pressure coupling are 0.1 ps and 0.5 ps, respectively. Long-range electrostatic interactions were calculated by the particle mesh Ewald (PME) method<sup>[32]</sup>. A cutoff radius of 1 nm for van der Waals and Coulomb interactions was used; the non-bonded pair list was updated every 10 steps. The integration time step was 2 fs and snapshots of the system were saved every 0.5 ps. The p29-p53 DBD complex was immersed in a cubic box filled with simple point charge (SPC) water<sup>[33]</sup> extending to at least 9 Å from the complex surface. A Na<sup>+</sup> ion was added to ensure the neutrality of the system. An energy minimization of 1000 steps using the steepest descent algorithm followed by 200 ps position restrained MD simulation, were carried out. Then, the system was heated by increasing the temperature from 50 K up to 300 K in 500 ps by steps of 50 K. The simulation at 300 K was carried out for 10 ns. The temporal evolution of the root mean square displacement (RMSD) and the root mean square fluctuations (RMSF) showed that the system was relaxed within the first 2 ns and remained stable during the following 8 ns. The values of C<sub>α</sub>-RMSD were generally below 3 Å. The coordinates of the complex at the end of the simulation were used for SMD (see Figure 1). The Hydrogen Bond (HB) analysis was

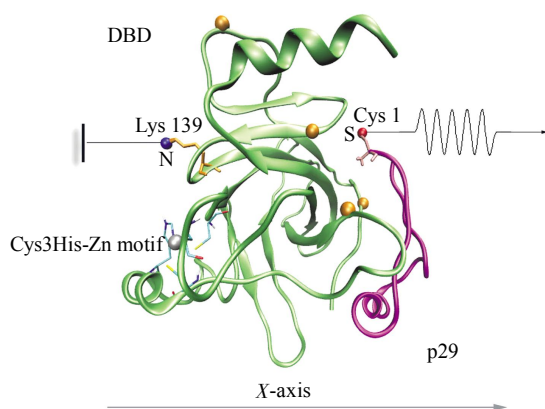


**Fig. 1** Molecular graphic representation of the starting configurations for the SMD runs for the p29-p53 DBD complex

The sulfur (S) of Cys1 of p29 is pulled, while the nitrogen (N) of Lys139 of p53 DBD is frozen. The residues and Zn in the Cys3His-Zn motif are shown with licorice model and sphere, respectively. Yellow balls on the backbone are the C<sub>α</sub> positions of lysines in p53 DBD except for Lys139.

carried out based on a geometric criterion for which the distance between acceptor and hydrogen is less than or equal to 0.3 nm and the angle between donor-hydrogen-acceptor is greater than or equal to 120°.

### 1.3 Steered MD

The SMD computational approach of the p28-p53 DBD complex was designed to closely match the AFS experimental setup used to investigate the same system<sup>[6]</sup>. In particular, the sulfur of an added cysteine residue to the p28 N-terminal, as previously described, was bound to a spring to mimic the binding of p28 to the AFM tip. At the same time, we selected as fixed atom of p53 DBD, the nitrogen atom of the lateral chain of Lys139 to miming the anchoring of p53 DBD to the substrate. The last choice was done by a preliminary screening of the available lysines on p53 DBD in order to check that the anchoring of p53 to the substrate does not alter its structure or it does not interfere with the formation of the complex. Among the five available lysine residues (Lys101, Lys120, Lys132, Lys139 and Lys164 of p53 DBD, marked as balls in Figure 1), Lys101, Lys132 and Lys164 were found as being close to the interface of the complex and then they were discarded. Similarly, Lys120 was discarded since its immobilization on the substrate could strongly hamper the complex formation. Although fixing a single atom could induce some stress in the pulled molecules<sup>[14, 34]</sup>, we preferred to use this setting to closely approach the experimental setup used on the AFS experiment on same system<sup>[6]</sup>. On the other hand, even other techniques, such as Surface Plasmon Resonance, require the fixing of molecules to a surface through single atoms<sup>[35]</sup>.

The equilibrated p28-p53 DBD complex was rotated in order to display the X-axis along the line joining the nitrogen of p53 DBD-Lys139 and the sulfur of p29-Cys1. Finally, the complex was centered in a rectangular box of 15.0 nm×7.0 nm×7.2 nm in size, filled with SPC water and equilibrated, as previously described. The SMD runs were carried out by keeping frozen the nitrogen of p53 DBD-Lys139, while the sulfur of p29-Cys1 bound to a spring was pulled along the positive direction of X-axis (see Figure 1) by a time-dependent external force with a constant speed  $v$ , according to:

$$F(t)=k(vt-\Delta x) \quad (1)$$

where the spring constant,  $k$ , was set to 100 kJ •mol<sup>-1</sup> •nm<sup>-2</sup> (~0.166 N/m), and  $\Delta x$  is the

$x$ -displacement of the pulled atom relative to its initial position.

Five values of pulling speed were investigated: 0.5, 1, 3, 5, 10 nm/ns. The simulation times were set to 18 ns for the slowest speed, 10 ns for the speed of 1 nm/ns and 5 ns for all the other pulling speeds to make sure that a complete unbinding was reached. For each pulling speed, five independent trajectories with different initial velocities were sampled. Fifteen more runs (twenty in total) have been carried out at the speed of 1 nm/ns for the calculation of the Potential of Mean Force (see below). All simulations and analysis were carried out on the high-performance computing (HPC) platform, at College of Computer Sciences, Beijing University of Technology. All figures of the protein structures were created by the VMD program<sup>[36]</sup>.

#### 1.4 Potential of mean force

The Potential of Mean Force (PMF), which provides the free energy profile along the reaction coordinate, was estimated from the SMD trajectories by using the Jarzynski's equality which establishes a relationship between the free energy,  $\Delta G$ , and the distribution of the work done along non-equilibrium paths connecting the initial and the final state, according to refs. <sup>[20-21]</sup>:

$$\langle e^{-\frac{W}{k_B T}} \rangle = e^{-\frac{\Delta G}{k_B T}} \quad (2)$$

where  $W$  is the work done by the applied force on the system (*i.e.* complex embedded into the solvent environment),  $k_B$  is the Boltzmann constant and  $T$  is the absolute temperature; the brackets denoting the average over unbinding trajectories with different starting states. The PMF profile was determined as a function of the reaction coordinate chosen as the distance between fixed and the pulled atom.

The work performed along each SMD trajectory was calculated by the approximated expression:

$$W(x) = \sum_i^{x_i \leq x} F(x_i)(x_i - x_{i-1}) \quad (3)$$

where  $x_i$  is the position of the pulled atom at the time  $t_i$ , and  $x_{i-1}$  is its position at the time  $t_i - t$ , with  $t$  being the time step;  $F(x_i)$  being the force applied at the pulled atom at the time  $t_i$ . The average and the corresponding standard deviation of  $W$ , at each position of the pulled atom, were calculated by taking

into account 18 independent SMD trajectories (selected from 20 runs).

A number of methods are available to construct the PMF from SMD simulations<sup>[37-39]</sup>. Here, we applied two different methods. First, the PMF profile was determined directly from Eq.2 through the work performed along each SMD trajectory and calculated by Eq.3 (called JE method). In addition, by assuming a Gaussian distribution of the work value, Eq.2 can be simplified using the second order cumulant expression<sup>[37]</sup>:

$$\Delta G = \langle W \rangle - \frac{\sigma_W^2}{2k_B T} \quad (4)$$

where  $\langle W \rangle$  is the mean value over all the trajectories and  $\sigma_W^2$  is the square standard deviation of the work distribution. In the cumulative integral (CI) extrapolation method, an integral is defined to take into consideration more accurate estimates of the free energy. Indeed, the CI method was shown to reduce the required data by 5 ~ 40 fold<sup>[38]</sup>. Calculations were carried out by the package <http://www.csb.pitt.edu/Faculty/zuckerman/software.html>.

## 2 Results and discussion

### 2.1 Unbinding pathway of the p53 DBD-p29 complex

Figure 2 shows the p53 DBD  $C_\alpha$ -RMSDs from the initial structure (averaged over both all the  $C_\alpha$ -atoms) as a function of time, for five runs with different initial conditions at the pulling speeds of 0.5, 3 and 10 nm/ns. The analyzed time intervals have been extended until the pulled molecule reaches the simulation box edge. At speed values of 0.5 and 3 nm/ns, the  $C_\alpha$ -RMSDs are characterized by both values below 0.2 nm with a rather low variability from run to run; this indicating that the structure of p53 DBD is substantially preserved during the SMD runs (Figure 2a and b). At higher pulling speeds, low  $C_\alpha$ -RMSD values are still obtained for some runs, however, drastic deviations appear in other runs; this being due to a partial unfolding observed in some runs (Figure 2c). Indeed, from an accurate inspection of the trajectories, we found that a distortion of the N-terminal region of p53 DBD located at the interface of the two partners, occasionally occurred.

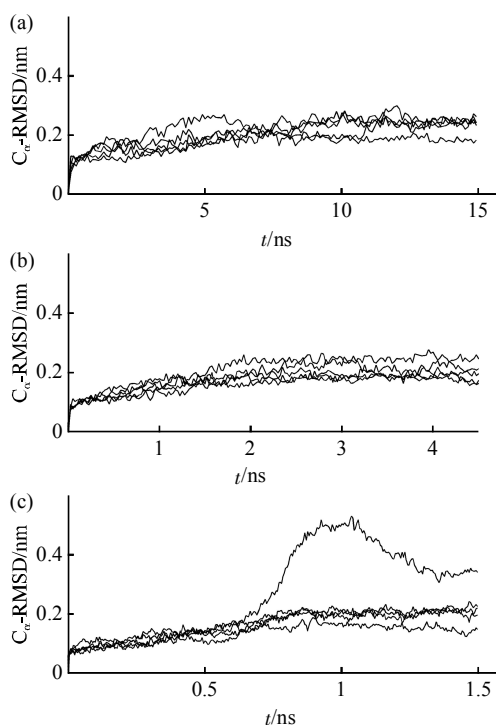


**Fig. 2** Temporal evolution of the  $C_{\alpha}$ -RMSD of the p53 DBD molecule involved in the p29-p53 DBD complex

Calculations are based on five independent SMD trajectories at pulling speeds of 0.5 nm/ns (a), 3 nm/ns (b) and 10 nm/ns (c).

The  $C_{\alpha}$ -RMSD values of the p29 peptide, shown in Figure 3, are below 0.2 nm again with a low variability from run to run for the lowest pulling speed. Instead, for higher speeds, quite large values of  $C_{\alpha}$ -RMSD are observed in some runs, as it emerges from the  $C_{\alpha}$ -RMSD temporal evolution at the pulling speed of 3 nm/ns shown in Figure 3. An inspection of

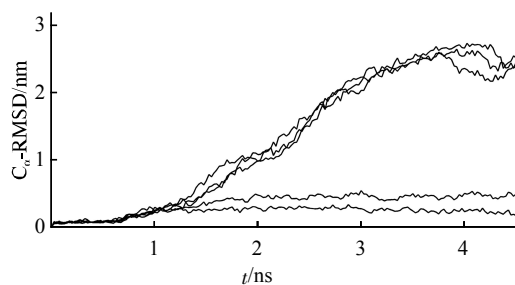


**Fig. 3** Temporal evolutions of the  $C_{\alpha}$ -RMSD of the p29 peptide involved in the p29-p53 DBD complex

Calculations are based on five independent SMD trajectories at pulling speed of 3 nm/ns.

the trajectories has revealed that such an increase is due to an opening of the loop formed by the N- and C-terminals of the peptide, with some distortion of its structure. Similar structural distortions and even unfolding processes have been observed in other SMD studies of biomolecular systems<sup>[14-15, 17]</sup>.

To quantitatively monitor the structural changes of the partners during the SMD runs, we have followed the temporal evolution of the distance between selected couples of atoms of the p29-p53 DBD complex. In particular, we have analyzed the following distances (see Figure 4a): (i)  $D1$ , between the  $C_{\alpha}$  of Ala6 and of Tyr24, which monitors the p29  $\beta$ -sheet conformation; and (ii)  $D2$ , between the  $C_{\alpha}$  of Val11 and of Ser18, which is a reporter on the p29  $\alpha$ -helix conformation. For pulling speeds below 1 nm/ns, we found that both  $D1$  and  $D2$  remain very close to the initial values during all the simulation, consistently with a preservation of both the peptide  $\alpha$ -helix structure and the  $\beta$ -sheet loop. At higher speed values, both the  $D1$  and  $D2$  distances may occasionally exhibit a significant deviation from their initial value. This is representatively shown in Figure 5 which refers to a pulling speed of 3 nm/ns. Figure 5a shows that  $D1$  and  $D2$  are almost constant during the runs, consistently with a preservation of the p29 structure during the pulling process. In other runs, both  $D1$  and  $D2$  strongly increase even exceeding 5 nm for  $D2$  (Figure 5b). Such an increase can be attributed to both an opening of the loop and a partial distortion of the  $\alpha$ -helix.

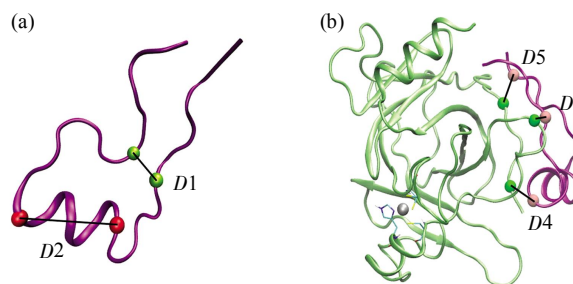


**Fig. 4** Selected residue pairs in peptide (a) and p29-p53 DBD complex (b)

(a) Molecular graphic representation of the initial structure of the p29 peptide involved in the p29-p53 DBD complex. The  $D1$  and  $D2$ , distances used to monitor the evolution of p29 along the SMD simulations, are marked as spheres and black lines. (b) Molecular graphic representation of the initial structure of the p53 DBD molecule involved in the p29-p53 DBD complex. The  $D3$ - $D5$  distances, chosen to monitor the evolution of the protein-protein interface during the unbinding process, are marked as spheres and black lines.

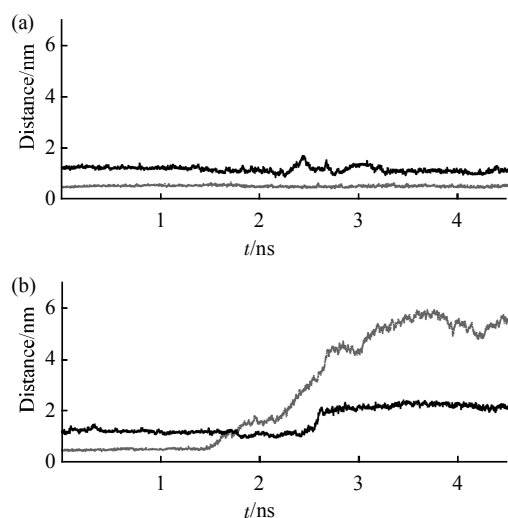


**Fig. 5** Temporal evolution of the *D1* (gray lines) and *D2* (black lines) distances

Calculations are based on SMD runs at the pulling speed of 3 nm/ns, for runs in which (a) the p29 structure is preserved and (b) p29 undergoes to a large unfolding. —: *D1*; —: *D2*.

The temporal evolution of the entire complex has been monitored by the following intermolecular distances (Figure 4b): (i) *D3* between the C<sub>α</sub>-Ser166 of p53 DBD and the C<sub>α</sub>-Ala5 of p29; (ii) *D4* between the C<sub>α</sub>-Val97 of p53 DBD and the C<sub>α</sub>-Gly10 of p29; and (iii) *D5* between the C<sub>α</sub>-Lys101 of p53 DBD and the C<sub>α</sub>-Asp28 of p29. We have separately analyzed the runs in which the peptide structure is preserved and those in which some distortion of p29 occurs.

Figure 6a shows the evolution for the *D3-D4-D5* distances which remain practically unchanged in the initial part of the runs and collected at a pulling speed of 3 nm/ns. At about 1 ns, *D5* starts to lengthen followed by the elongation of *D3* and then of *D4*. The same qualitative sequence has been also observed in the runs performed at the other pulling speeds, even if the departure from the initial values takes place at slightly different times (not shown). Anyway, the unbinding of the p29-p53 DBD complex mainly follows a candidate pathway in which the elongation of *D5* is followed by that of *D3*, and finally of *D4* (*D5-D3-D4* sequence). This means that the detachment of p29 from p53 DBD starts with the escape of both its C-terminal and β-sheet regions from the interface, followed by that of its α-helix (Movie S1 in Supplementary Material).

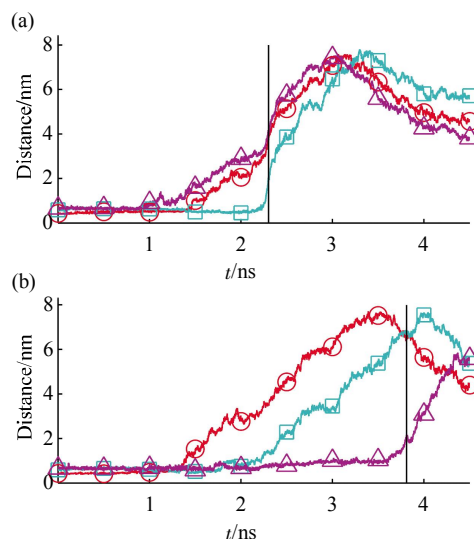


**Fig. 6** Temporal evolutions of the distances *D3* (circle), *D4* (square) and *D5* (triangle)

Calculations are based on the SMD runs for the p29-p53 DBD complex at the pulling speed of 3 nm/ns, for runs in which: (a) the p29 structure is preserved; and (b) p29 undergoes to a large unfolding. The lines mark the time at which the unbinding of the complex has been just completed (see the text). The data have been obtained from the same SMD runs in Figure 5. ○—○: *D3*; □—□: *D4*; △—△: *D5*.

The evolution of *D3-D4-D5* distances for runs during which p29 undergoes a significant distortion, is shown in Figure 6b. *D3* starts to increase at about 1.4 ns, followed by an increase of *D4* and then of *D5*. Accordingly, the contacts between the C-terminal of p29 and p53 DBD remain stable while the N-terminal of p29 detaches from p53 DBD, with a concomitant opening of the loop and a separation of the strands. Successively the p29 α-helix, which is partially distorted as witnessed by the increase of *D2* (see Figure 5b), begins to depart from the p53 DBD interface as monitored by the increase of *D4*. The lengthening of *D5* indicates that the p29 C-terminal escapes from the surface of p53 DBD after the opening of the p29 loop (Movie S2 in Supplementary Material).

Interestingly, about a 85% of the total runs is characterized by a preservation of the p29 structure irrespectively of the applied pulling speed value. In these runs, the detaching of the molecules follows a candidate pathway as monitored by the *D3-D4-D5* distances.

To evaluate the time at which the unbinding process of the complex has been just completed, we

have assumed that the unbinding occurs when the distance between all the  $C_{\alpha}$ -atoms of p53 DBD from those of p29 overcomes the threshold of 1.3 nm<sup>[15, 17]</sup>. Such a time has been indicated with a vertical line in Figure 6. The unbinding is observed at shorter times in the runs during which p29 undergoes to a partial unfolding with respect to those during which p29 preserves its structure. Furthermore, unbinding is completed within shorter times when higher pulling speeds are applied (not shown).

We have also analyzed the behavior of the intermolecular hydrogen bonds (HBs) network whose formation and dynamics can play a crucial role in driving the approach between the molecules and the stabilization of the complex. Figure 7 shows the temporal evolution of the total number of hydrogen bonds (HBs) between the two partners for the same runs analyzed in Figure 5 and 6. For a comparison, the temporal evolution of the total number of intermolecular HBs from simulations at equilibrium (*i.e.* without any applied force) have been also shown (gray lines). We note that the total number of

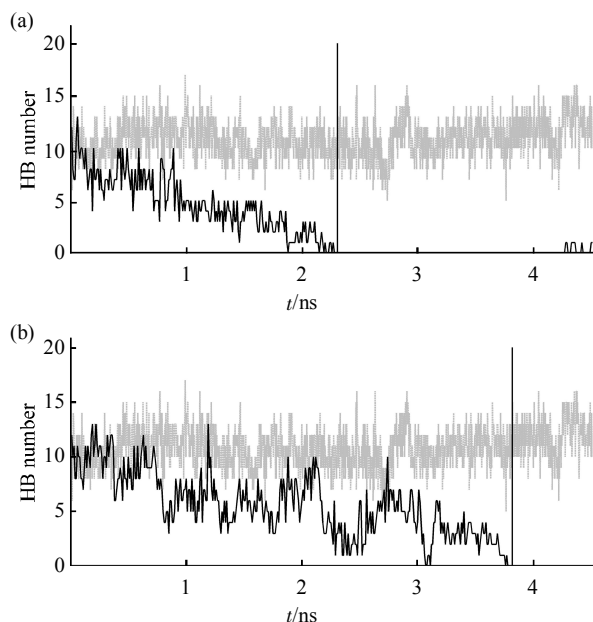


**Fig. 7** Temporal evolution of the number of the intermolecular HBs formed within the p29-p53 DBD complex

Calculations are based on a SMD run at a pulling speed of 3 nm/ns (black lines). (a) the p29 structure is preserved; and (b) p29 undergoes to a large unfolding. Data have been obtained from the same runs used in Figure 5. For comparison, the temporal evolution of the HB number between p53 DBD and p29 during a simulation run without any applied force is also shown (gray lines). The lines mark the time at which the unbinding of the complex has been just completed (see the text).

intermolecular HBs initially fluctuates around 10, and then it progressively decreases to zero; the same trend to zero having been observed in all the runs.

Interestingly, the HB number starts to decrease with respect to the initial values at the very beginning of the run. This indicates that the pulling process yields a progressive weakening of the HB intermolecular network, even if a detachment of the partners is not yet evident (see Figure 6). The HB number decreases to zero within 2.5 ns in all the runs during which the p29 structure remains almost stable, while it goes to zero within longer times (up to 4 ns) for runs displaying some unfolding of p29 (see Figure 6). It is interesting to note that the breaking of all the intermolecular HBs practically coincides with the unbinding (see the lines marking the unbinding in Figure 7); such a coincidence having been registered also for other runs. A significant acceleration of the rupture of the HB network has been observed for higher pulling speeds (not shown), consistently with a faster unbinding at higher applied forces.

In summary, we found that, when low pulling speeds are applied, p29 detaches from p53 DBD by substantially preserving its folding and the system follows an unbinding pathway characterized by increasing intermolecular distances with a well established sequence (*D5-D3-D4*). These results put into evidence the intermolecular contact points which regulate and stabilize the formation of the complex and it may be of some help to refine the structure of the peptide to improve its binding capability. The occasional observation of a partial distortion of the p29 peptide during the pulling, at high speed values, suggests to take into consideration essentially on data coming from SMD at low pulling speed.

## 2.2 Energy landscape of the p29-p53 DBD complex unbinding

The equilibrium parameters related to the kinetics of the complex formation, and information on the energy landscape of the unbinding process, can be extracted from the inherently non-equilibrium SMD simulations, by means of appropriate theoretical approaches<sup>[35]</sup>. First, we have analyzed the temporal evolution of the force applied to the complex at the various pulling speeds. In the following, we have restricted our analysis to the SMD runs where both the p53 DBD and the p29 molecule preserve their structure during the unbinding process. We note that the force applied to the system is expected to induce

the unbinding of the complex through a progressive breaking of the intermolecular (non-covalent) bonds and, at the same time, to drive the diffusion of the pulled molecule through the solvent environment<sup>[15]</sup>. Figure 8 shows the temporal trend of the applied forces at the pulling speeds of 0.5, 3 and 10 nm/ns. At each speed, two curves corresponding to different initial conditions, have been shown. In all the cases, the applied force increases up to a maximum after which it shows a steep decrease which is more abrupt at lower pulling speeds. For each curve shown in Figure 8, we have labeled with a vertical line the time at which the unbinding process has been just completed, according to the criterion assumed in the previous Section. These times are mainly located in the initial part of the downhill region after the force curve maximum, similarly to what observed in other works<sup>[29]</sup>. In this respect, we remark that to extract the unbinding force from the trend of the force during the SMD different criteria have been developed and applied. Mainly, it has been assumed that the unbinding of the complex occurs just in correspondence of the maximum of the force curves<sup>[10]</sup>. However, although the maximum is

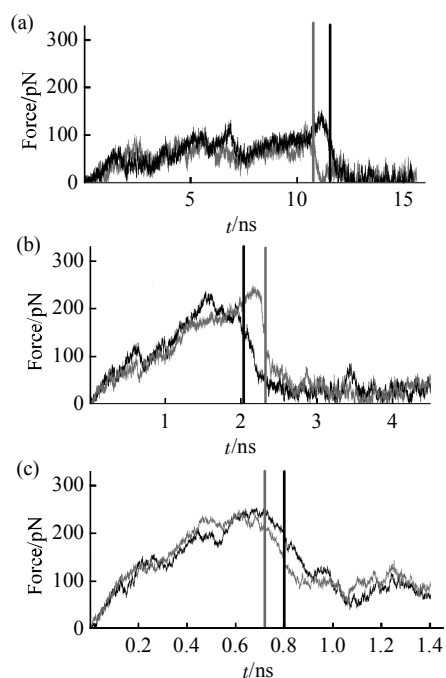


**Fig. 8 Temporal evolution of the applied forces on the p29-p53 DBD complex during SMD simulations**

The data are from SMD runs at pulling speeds of 0.5, 3 and 10 nm/ns. For each speed, the force evolution from two different trajectories has been shown (black and grey lines). The lines mark the time at which the unbinding of the complex has been just completed (see the text).

related to the rupture of important contacts between the partners, we found that it does not necessarily correspond to the achievement of a complete unbinding of the complex, as also observed in our case.

Furthermore, we have compared our SMD force curves with the force curves obtained in AFS experiments<sup>[7]</sup>. Figure 9 shows the force values of Figure 8b (gray line) plotted as a function of the distance between the frozen and the pulled atoms. The curve shows an initial increasing trend followed by a rather abrupt decrease after which the force remains almost constant. The occurrence of the unbinding event along the rapid decrease (see the cross in Figure 9) finds a close correspondence with the so-called jump-off in the AFS force curve<sup>[27]</sup>.

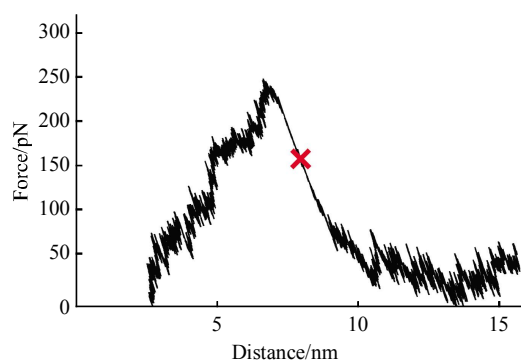


**Fig. 9 The plot of force as a function of the distance between the frozen atom and the pulled atom**

The data is based on the same trajectory used in Figure 8b (gray line). The cross marks the point at which the unbinding of the complex has been just completed.

For each pulling speed, we have considered as the unbinding force ( $F^*$ ), that one corresponding to the time at which the unbinding process is complete. These unbinding forces range between 50 and 400 pN, with higher values occurring at faster pulling speed; values in the same range having been observed in other SMD studies of biomolecular complexes<sup>[10, 15, 17]</sup>.

As already mentioned, the unbinding force value encompasses a component necessary to move the pulled molecule throughout the solvent environment to overcome frictional effects. This force component ( $F_{\text{fric}}$ ) can be evaluated from the last part of the SMD trajectories where the pulled molecule moves in the solvent beyond its complete unbinding from the

partner (Neumann and Gottschalk, 2009). We found that the estimated frictional forces are almost zero at the lowest pulling speed, while they increase significantly at high pulling speed values, in agreement with the velocity dependence of frictional forces. Accordingly, the effective unbinding force,  $F_{\text{unb}}$ , required to unbind the p29-p53 DBD complex, has been determined by subtracting this frictional force from the unbinding force ( $F_{\text{unb}} = F^* - F_{\text{fric}}$ ).

The plot of the effective unbinding force ( $F_{\text{unb}}$ ) as a function of the logarithm of the pulling speed, shown in Figure 10, follows an almost linear trend similarly to what found in other SMD works<sup>[17, 40]</sup>. Notably, such a trend is also reminiscent of that generally found in AFS works for different complex including the p53 DBD-p28<sup>[35]</sup>. Although the observed linear trend, in principle, could be interpreted in terms of the Bell-Evans model which underlies the existence of a single barrier to be overcome during the unbinding process, the stiffness of the used spring together with the rather high pulling speed values, do not allow us for extrapolating the SMD data to experimental timescales in a reliable way<sup>[17-18, 40]</sup>.

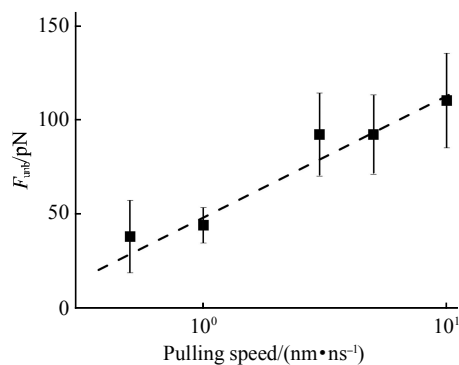


**Fig. 10 Effective unbinding force for the p29-p53 DBD complex plotted as a function of the logarithm of the pulling speed**

Each value of the unbinding force has been averaged over five runs with different initial conditions; the corresponding standard deviations being shown as error bars.

We have finally evaluated the binding free energy profile along a reaction coordinate by applying the Jarzynski's equality. Such a theoretical approach allows ones to determine the free energy of a reaction (here the unbinding process) at equilibrium from a collection of the irreversible works performed during the unbinding paths in nonequilibrium conditions. As

described in the Method Section, we have evaluated the PMF by the two different approaches. Figure 11 shows the PMF as a function of the reaction coordinate at the pulling speed of 1 nm/ns, evaluated from the JE (black line) and from the CI method (red line). In both cases, the PMF increases up to reach a maximum following practically the same trend. After the maximum, the PMF from the JE method appears almost constant, while a slight decrease is detected for the CI method. The satisfactory agreement between the approaches is consistent with the fact that the distribution of the work can be satisfactorily described by a Gaussian distribution (see the inset of Figure 11). From the trend of the PMF the binding free energy can be evaluated from the PMF value in correspondence to the unbinding. By taking into consideration the previously described criterion, the unbinding free energy can be extracted the reaction coordinate is about 8.9 nm (see the arrow in Figure 11). We found an unbinding free energy  $G$  of 82 kcal/mol and of 74 kcal/mol can be extracted from the PMF by the JE and CI approaches, respectively. Although such a value is rather high, we note that similar values have been obtained for other complexes from SMD runs<sup>[41]</sup>. Additionally, the binding free energy determined from SMD is lower than that evaluated by an approach conjugating MD simulation and rigid docking ( $150 \pm 30$ ) kcal/mol<sup>[5]</sup>. Such an overestimation could be attributed to the force field used in both our simulations.

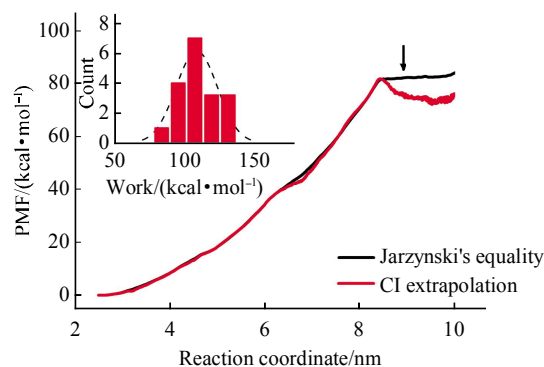


**Fig. 11 PMF as a function of the reaction coordinate for the p29-p53 DBD complex**

The reaction coordinate is given by the distance between the fixed and the pulled atom. PMF are evaluated by the JE method (black line) and CI (red line) extrapolation method. The arrow marks the time at which the unbinding of the complex has been just completed (see the text). The calculations were based on 18 different SMD trajectories at the pulling speed of 1 nm/ns. Inset: distribution of the work performed on the system and a fit by a Gaussian distribution (dashed line).

### 3 Conclusions

The SMD approach applied to the complex formed between the p53 DBD portion of the tumor suppressor p53 and the p28 anticancer peptide has allowed us to elucidate its unbinding process at atomic level. We found that the unbinding of the p28 peptide from the p53 DBD takes place by following a candidate detaching path, involving the C-terminal followed by the  $\beta$ -sheet and by the  $\alpha$ -helix of p28; such a path appearing to be independent on both the pulling speeds and initial conditions. The persistence of the possible unbinding path indicates which intermolecular contact points play the most important role in the stabilizing the formation of the complex. In addition, we found that, while the p28 peptide preserves its structure during the pulling upon applying low pulling speed values, at high speed it may undergo to some unfolding. An analysis of the unbinding forces in the framework of the Jarzynski's equality, has allowed us to determine the work and the PMF profile of the free energy profile of the unbinding process for the p28-p53 DBD complex. These results can be useful in the understanding of the molecular key regulating the biorecognition mechanisms between the p53 DBD and the anticancer p28 peptide. Accordingly, they can provide some help to refine drugs with an improved binding capability and likely with an enhanced anticancer activity.

**Supplementary material** Movie S1 and S2, are available at PIBB website(<http://www.pibb.ac.cn>).

### References

- [1] Taylor B N, Mehta R R, Yamada T, *et al.* Noncationic peptides obtained from azurin preferentially enter cancer cells. *Cancer Res*, 2009, **69**(2): 537–546
- [2] Yamada T, Mehta R R, Lekmine F, *et al.* A peptide fragment of azurin induces a p53-mediated cell cycle arrest in human breast cancer cells. *Mol Cancer Ther*, 2009, **8**(10): 2947–2958
- [3] Mehta R R, Hawthorne M, Peng X, *et al.* A 28-amino-acid peptide fragment of the cupredoxin azurin prevents carcinogen-induced mouse mammary lesions. *Cancer Prev Res*, 2010, **3**(10): 1351–1360
- [4] Oren M. Decision making by p53: life, death and cancer. *Cell Death Diff*, 2003, **10**(4): 431–442
- [5] Santini S, Bizzarri A R, Cannistraro S. Modelling the interaction between the p53 DNA-binding domain and the p28 peptide fragment of Azurin. *J Mol Recognit*, 2011, **24**(6): 1043–1055
- [6] Bizzarri A R, Santini S, Coppari E, *et al.* Interaction of an anticancer peptide fragment of azurin with p53 and its isolated domains studied by atomic force spectroscopy. *Int J Nanomed*, 2011, **6**: 3011–3019
- [7] Bizzarri A R, Cannistraro S. Atomic force spectroscopy in biological complex formation: strategies and perspectives. *J Phys Chem B*, 2009, **113**(52): 16449–16464
- [8] Bizzarri A R, Cannistraro S. The application of atomic force spectroscopy to the study of biological complexes undergoing a biorecognition process. *Chem Soc Rev*, 2010, **39**(2): 734–749
- [9] Rief M, Grubmüller H. Force spectroscopy of single biomolecules. *Chemphyschem*, 2002, **3**(3): 255–261
- [10] Bayas M V, Schulten K, Leckband D. Forced detachment of the CD2-CD58 complex. *Biophys J*, 2003, **84**(4): 2223–2233
- [11] Niu C Y, Xu Y C, Xu Y, *et al.* Dynamic mechanism of E2020 binding to acetylcholinesterase: a steered molecular dynamics simulation. *J Phys Chem B*, 2005, **109**(49): 23730–23738
- [12] Liu X L, Xu Y C, Wang X C, *et al.* Unbinding of nicotine from the acetylcholine binding protein: steered molecular dynamics simulations. *J Phys Chem B*, 2008, **112**(13): 4087–4093
- [13] Morfill J, Neumann J, Blank K, *et al.* Force-based analysis of multidimensional energy landscapes: application of dynamic force spectroscopy and steered molecular dynamics simulations to an antibody fragment-peptide complex. *J Mol Biol*, 2008, **381**(5): 1253–1266
- [14] Cuendet M A, Michielin O. Protein-protein interaction investigated by steered molecular dynamics: The TCR-pMHC complex. *Biophys J*, 2008, **95**(8): 3575–3590
- [15] Neumann J, Gottschalk K E. The effect of different force applications on the protein-protein complex barnase-barstar. *Biophys J*, 2009, **97**(6): 1687–1699
- [16] Guzman D L, Randall A, Baldi P, *et al.* Computational and single-molecule force studies of a macro domain protein reveal a key molecular determinant for mechanical stability. *Prog Natl Acad Sci USA*, 2010, **107**(5): 1989–1994
- [17] Bizzarri A R. Steered molecular dynamics simulations of the electron transfer complex between azurin and cytochrome c(551). *J Phys Chem B*, 2011, **115**(5): 1211–1219
- [18] Izrailev S, Stepaniants S, Balsera M, *et al.* Molecular dynamics study of unbinding of the avidin-biotin complex. *Biophys J*, 1997, **72**(4): 1568–1581
- [19] Hummer G, Szabo A. Kinetics from nonequilibrium single-molecule pulling experiments. *Biophys J*, 2003, **85**(1): 5–15
- [20] Lorenzo A C, Bisch P M. Analyzing different parameters of steered molecular dynamics for small membrane interacting molecules. *J Mol Graph Model*, 2005, **24**(1): 59–71
- [21] Jarzynski C. Nonequilibrium equality for free energy differences. *Phys Rev Lett*, 1997, **78**(14): 2690–2693
- [22] Jarzynski C. Equalities and inequalities: irreversibility and the second law of thermodynamics at the nanoscale. *Annu Rev Condens Matter Phys*, 2011, **2**: 329–351
- [23] Cho Y, Gorina S, Jeffrey P D, *et al.* Crystal structure of a p53 tumor suppressor-DNA complex: understanding tumorigenic mutations.

- Science, 1994, **265**(5170): 346–355
- [24] Calimet N, Simonson T. Cys(x)His(y)-Zn<sup>2+</sup> interactions: possibilities and limitations of a simple pairwise force field. *J Mol Graph Model*, 2006, **24**(5): 404–411
- [25] Guex N, Peitsch M C. SWISS-MODEL and the Swiss-PdbViewer: An environment for comparative protein modeling. *Electrophoresis*, 1997, **18**(15): 2714–2723
- [26] Hess B, Kutzner C, van der Spoel D, *et al.* GROMACS 4: Algorithms for highly efficient, load-balanced, and scalable molecular simulation. *J Chem Theory Comput*, 2008, **4**(3): 435–447
- [27] Van der Spoel D, Lindahl E, Hess B, *et al.* GROMACS: Fast, flexible, and free. *J Comput Chem*, 2005, **26**(16): 1701–1718
- [28] van Gunsteren W F, Billeter S R, Eking A A, *et al.* Biomolecular Simulation, The GROMOS96 Manual and User Guide. Vdf Hochschulverlag AG an der ETH Zürich, Zürich, Switzerland., 1996
- [29] Hess B, Bekker H, Berendsen H J C, *et al.* LINCS: a linear constraint solver for molecular simulations. *J Comput Chem*, 1997, **18**(12): 1463–1472
- [30] Bussi G, Donadio D, Parrinello M. Canonical sampling through velocity rescaling. *J Chem Phys*, 2007, **126**(1): 014101
- [31] Parrinello M, Rahman A. Polymorphic transitions in single- crystals - a new molecular-dynamics method. *J Appl Phys*, 1981, **52**(12): 7182–7190
- [32] Essmann U, Perera L, Berkowitz M L, *et al.* A smooth particle mesh ewald method. *J Chem Phys*, 1995, **103**(19): 8577–8593
- [33] Berendsen H J C, Grigera J R, Straatsma T P. The missing term in effective pair potentials. *J Phys Chem*, 1987, **91**(24): 6269–6271
- [34] Colizzi F, Bussi G. RNA Unwinding from reweighted pulling simulations. *J Am Chem Soc*, 2012, **134**(11): 5173–5179
- [35] Bizzarri A R, Cannistraro S. *Dynamic Force Spectroscopy and Biomolecular Recognition*. CRC Press, Boca Raton: 2012
- [36] Humphrey W, Dalke A, Schulten K. VMD: Visual molecular dynamics. *J Mol Graph Model*, 1996, **14**(1): 33–38
- [37] Park S, Khalili-Araghi F, Tajkhorshid E, *et al.* Free energy calculation from steered molecular dynamics simulations using Jarzynski's equality. *J Chem Phys*, 2003, **119**(6): 3559–3566
- [38] Ytreberg F M, Zuckerman D M. Efficient use of nonequilibrium measurement to estimate free energy differences for molecular systems. *J Comput Chem*, 2004, **25**(14): 1749–1759
- [39] Zhang D Q, Gullingsrud J, McCammon J A. Potentials of mean force for acetylcholine unbinding from the alpha7 nicotinic acetylcholine receptor ligand-binding domain. *J Am Chem Soc*, 2006, **128**(9): 3019–3026
- [40] Heymann B, Grubmuller H. AN02/DNP-hapten unbinding forces studied by molecular dynamics atomic force microscopy simulations. *Chem Phys Lett*, 1999, **303**(1–2): 1–9
- [41] Yu R, Kaas Q, Craik D J. Delineation of the unbinding pathway of alpha-conotoxin ImI from the alpha7 nicotinic acetylcholine receptor. *J Phys Chem B*, 2012, **116**(21): 6097–6105

# p53 DNA 结合域与抗癌多肽的 拉伸分子动力学研究 \*

许先进<sup>1)</sup> 苏计国<sup>2)</sup> 陈慰祖<sup>1)</sup> 王存新<sup>1)\*\*</sup> CANNISTRARO Salvatore<sup>3)</sup>  
BIZZARRI Anna-Rita<sup>3)\*\*</sup>

<sup>1)</sup>北京工业大学生命科学与生物工程学院, 北京 100124;

<sup>2)</sup>燕山大学理学院, 秦皇岛 066004;

<sup>3)</sup>*Biophysics and Nanoscience Center, Department of Ecology and Biology (DEB), University of Tuscia, 01100 Viterbo, Italy)*

**摘要** 研究发现, 取自蓝铜蛋白 azurin 的一段多肽 p28 能够进入癌细胞, 结合到肿瘤抑制因子 p53 的 DNA 结合域上, 进而增加 p53 的抗癌能力. 本工作中, 通过拉伸分子动力学方法, 在原子尺度上研究了 p28-p53 DBD 复合物的解离过程. 分析结果显示复合物的解离过程遵循着一定的分离顺序. 对解离力的分析以及对沿着解离路径的不可逆做功的计算, 使我们能够从复合物的能量地貌中提取有用的信息, 而这些信息也决定了复合物的解离过程.

**关键词** 拉伸分子动力学, p53, 抗癌多肽

**学科分类号** Q6, Q51

**DOI:** 10.3724/SP.J.1206.2013.00294

---

\* 科技部国际合作项目(2010DFA31710), 国家自然科学基金(11204267)和北京工业大学博士生创新基金和意大利癌症研究协会(IG 10412)资助项目.

\*\* 通讯联系人.

王存新. Tel: 010-67392724, E-mail: cxwangbjut@gmail.com

BIZZARRI Anna-Rita. Tel: 39-761-357031, E-mail: bizzarri@unitus.it

收稿日期: 2013-06-24, 接受日期: 2013-12-09